EDFAAO (2017) 4:12-20 1537-0755/$19.00 ©ASM International®

NANOSCALE CAPACITANCE AND CAPACITANCE-VOLTAGE CURVES FOR ADVANCED CHARACTERIZATION OF ELECTRICAL PROPERTIES OF SILICON AND GaN STRUCTURES USING SCANNING MICROWAVE IMPEDANCE MICROSCOPY (sMIM)

Oskar Amster, Stuart Friedman, Yongliang Yang, and Fred Stanke
PrimeNano, Inc.
amster@primenanoinc.com

OVERVIEW

A relatively new electrical mode, scanning microwave impedance microscopy (sMIM), measures a material's change in permittivity and conductivity at the scale of tens of nanometers.[1] The use of atomic force microscopy (AFM) electrical measurement modes is a critical tool for the study of semiconductor devices and process development. More specifically, the application of AFM electrical modes is an important tool for characterizing semiconductor devices during process development and failure analysis. The AFM-based electrical measurement techniques, such as scanning capacitance microscopy (SCM) and scanning spreading-resistance microscopy,[2,3] have shown value for dopant profiling in semiconductor samples with sub-50 nm spatial resolution. However, there has been no single scanning probe technique capable of quantifying at submicron dimensions the local electrical properties of materials (dielectric constant and conductivity) with the sensitivity and dynamic range required by the semiconductor industry and research communities.

Scanning microwave impedance microscopy provides the capability to directly probe a sample's permittivity and conductivity at submicron geometries. Scanning microwave impedance microscopy provides the real and imaginary impedance (Re(*Z*) and Im(*Z*), respectively) of the probe-sample interface impedance. By measuring the reflected microwave signal as a sample of interest imaged with an AFM, one can capture in parallel the variations in permittivity and conductivity and, for

"SCANNING MICROWAVE IMPEDANCE MICROSCOPY PROVIDES THE CAPABILITY TO DIRECTLY PROBE A SAMPLE'S PERMITTIVITY AND CONDUCTIVITY AT SUBMICRON GEOMETRIES."

doped semiconductors, the variations in depletion-layer geometry.[4,5] Scanning capacitance microscopy, an existing technique for characterizing doped semiconductors, modulates the tip-sample bias and detects the tip-sample capacitance with a lock-in amplifier. A previous study compared sMIM to SCM and highlighted the additional capabilities of sMIM,[6,7] including examples of nanoscale capacitance-voltage curves.

The initial implementation of sMIM focused on the relative measurement of local permittivity and conductivity at a sample surface. The capability to directly image the local variation of a sample's electrical properties at tens of nanometers has stimulated new areas of research. For technologically and scientifically interesting materials, such as graphene,[8] carbon nanotubes,[9] ferroelectric domains,[10,11] and doped semiconductors,[12-14] researchers are actively using this technique to gain new understanding of materials systems behavior.

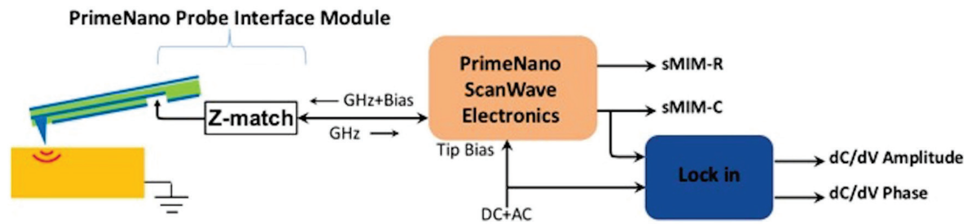

Fig. 1 **Schematic of the PrimeNano ScanWave electronics, matching circuit with shielded coaxial line to the probe-sample interface**

The natural progression and general interest in the user community is to extend the sMIM capabilities to quantitative measurements. This article presents recent analytical and finite-element modeling developments of tip-bias-dependent depletion-layer geometry and impedance. These are compared to experimental results on reference samples for both silicon- and GaN-doped staircases to systematically validate the response of the sMIM-C channel to the doping concentration.

INTRODUCTION

In a standard sMIM experiment, microwaves are coupled through a custom AFM cantilever to the probe tip, where they interact as evanescent waves with the portion of the sample immediately under the tip. A fraction of the microwaves is reflected, and the amplitude and phase (or equivalently, the real and imaginary parts) of the reflection are determined by the local electrical properties of the sample. For a linear sample (e.g., a dielectric or metallic material), the permittivity and conductivity determine the reflection, while for a nonlinear sample (e.g., a doped semiconductor), the tip-bias-dependent depletion-layer structure contributes significantly. As a result, sMIM measurements can provide valuable nanoscale information about semiconductor devices, processes, and defects.

A custom AFM probe is mounted in a specialized holder so that there is a coaxial connection from the microwave source to the AFM probe tip. The specialized probe module with matching circuit is then fitted to a standard AFM. The AFM typically operates in contact mode for imaging but can also be used in intermittent and tapping modes. The sMIM probes contain a multilayer cantilever with a shielded signal line connecting a contact pad on the carrier chip to the metallic tip at the end of the cantilever. The holder connects to the contact pad and couples 3 GHz microwaves from the sMIM measurement electronics to the AFM probe carrier chip, where they propagate along the signal line in the cantilever to the conductive tip.[15] The reflected signal retraces the same path. This configuration is illustrated schematically in Fig. 1. The probes, probe interface module, and electronics are part of a commercial ScanWave sMIM module (PrimeNano, Inc.). The sMIM is adapted to the most common commercial AFM platforms.[4,5]

The sMIM-C measured on various bulk dielectrics shows a clear linear relationship between sMIM-C and the log of the permittivity.[4,5,16] The red squares shown in Fig. 2 are from a model that originates with a finite-element calculation of the tip-sample admittance for the conical geometry of the sMIM probe. The origins of the log(ε) dependence can be seen in analytical models for spherically terminated conical tips above and in contact with linear materials, documenting the origin of the log dependence published by other researchers.[17]

For sMIM measurements on nonlinear materials, such as a doped semiconductor, the tip-sample bias influences the tip-sample impedance, or, more conveniently, the reciprocal of the tip-sample impedance, the tip-sample admittance, $Y_{T\text{-}S}$. As with linear samples, the sMIM signals are still proportional to the imaginary and real parts of $Y_{T\text{-}S}$, the capacitance and conductance below the tip-sample interface, but the capacitance and conductance now depend not only on the local permittivity and conductivity of the sample under the tip but also on the geometry of

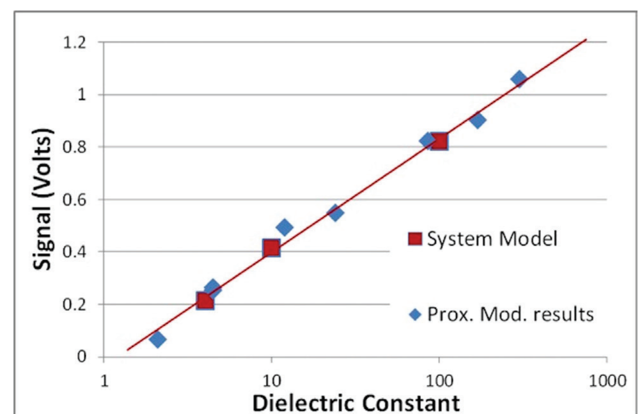

Fig. 2 **Graph of the numerically modeled admittance versus the dielectric value (in red) with the experimentally measured sMIM versus the dielectric value (in blue) from a group of bulk crystal dielectric samples**

the depletion layer. The depletion-layer geometry, in turn, depends on the tip-sample direct current or low-frequency voltage and on the doping level of the semiconductor. Analytical solutions exist for one-dimensional geometries, and these can be used to model the results from macroscopic parallel-plate metal oxide semiconductor (MOS) structures. Figure 3 shows the classic parallel-plate model for describing a MOS device. A lumped-element approximation for an sMIM tip on an oxide-coated semiconductor and expressions from the delta depletion model for depletion-layer thickness[17] are shown in Fig. 3.

Because depletion-layer geometry has a strong impact on sMIM signals and because the depletion-layer geometry varies with tip-sample voltage and with doping, varying the tip-sample voltage is a way to characterize semiconductor materials and devices, particularly the local

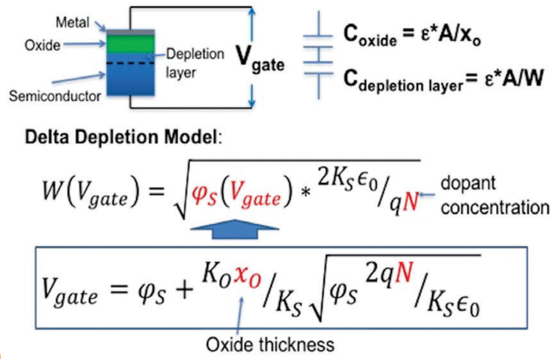

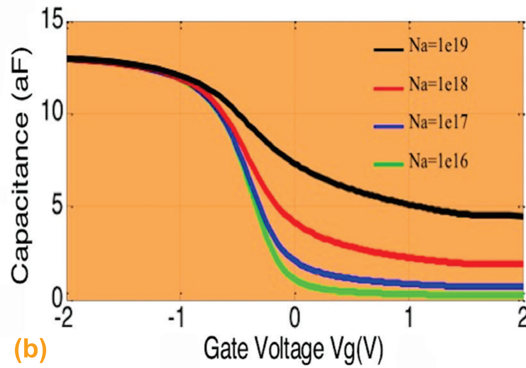

Fig. 3 **(a) Schematic of the classical MOS device configuration with the sMIM probe contacting a sample surface modeled as two series capacitors. The equations describe the relationship of the capacitance (and therefore the sMIM) measurement on the depletion-layer thickness and doping concentration. (b) Numerically generated capacitance-voltage curves from the parallel-plate model illustrate sMIM's sensitivity to semiconductor doping level.**

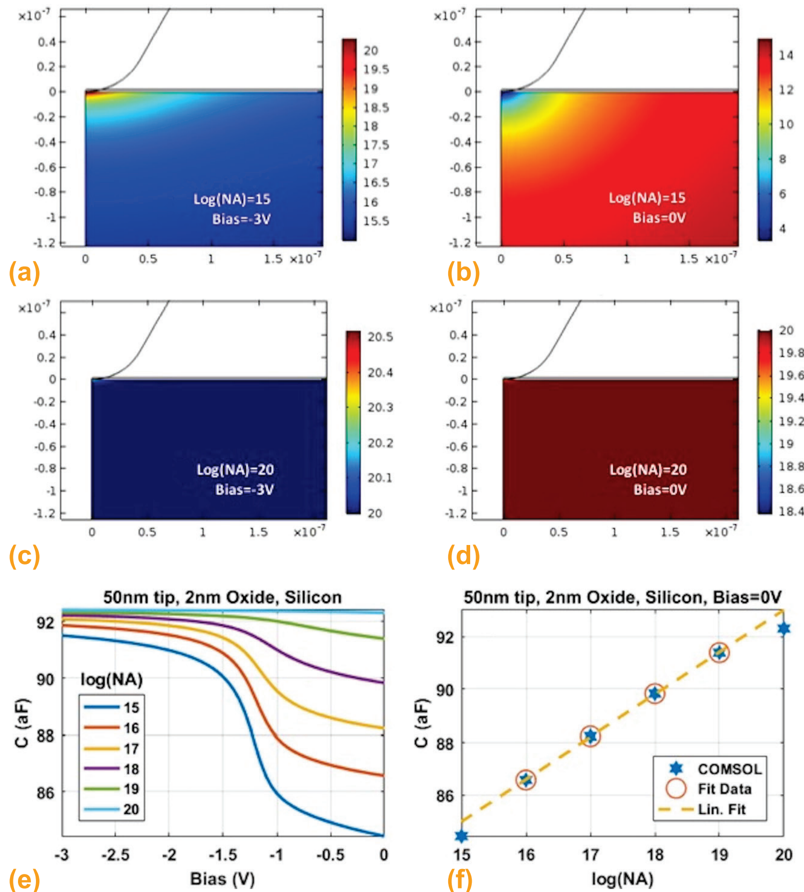

Fig. 4 **(a-d) Finite-element model (FEM) predictions of the majority carrier hole density in the presence of marked biases on an sMIM probe for the marked *p*-type doping densities in silicon. Many more such simulations led to (e) FEM predictions of C-V curves, with the dopings specified by the legend. (f) Calibration of the probe tip's capacitance over the various doped samples as a function of their doping density**

doping level under the tip (or electrode, in the case of patterned samples with electrodes present). This is similar to capacitance-versus-voltage curves from macroscopic samples commonly used to characterize semiconductor materials and test structures. Figure 3(b) presents the classical solution to the parallel-plate model, numerically generated here for a range of doping concentration levels. This model is incomplete for describing the geometries for AFM probe-sample interactions.

Similar to what was observed in the measurements of linear dielectrics shown in Fig. 2, where the sMIM signal is proportional to log(ε), experimental data from doped semiconductors show sMIM signals varying linearly with log([doping concentration]). To confirm the origins of the log([doping concentration]) behavior, finite-element modeling was used to assess the depletion-layer geometry for a conical tip and how this geometry varies for both doping and applied gate (i.e., tip) voltage. Figure 4(a) shows the results for one doping level.

The finite-element models also allow calculation of the tip-sample capacitance for each doping level and gate voltage, resulting in capacitance-voltage (C-V) curves for the geometry of an sMIM probe on an oxide-coated semiconductor (Fig. 4e). Experimental data presented subsequently in this article resemble the model results, indicating that most critical physics are accounted for by the models. Figure 4(f) shows that the capacitance seen and measured by sMIM is linear in log doping over several orders of magnitude for dopings of practical importance, enabling the possibility of calibrating sMIM results to invert for doping density.

EXAMPLES OF sMIM AND C-V ON SILICON SAMPLES

It has been shown in previous work[4,5] that sMIM-C is linear with the log N_A. Results presented in this section show application of sMIM-C's linear relationship to log N_A for quantification of sMIM-C doping concentration in log units. An IMEC *n*-type doped staircase was used as a calibration sample. The IMEC staircase is measured using ScanWave sMIM to determine a calibration curve that can then be applied to an unknown sample to convert sMIM-C to units of doping concentration. Figure 5(a) shows the sMIM-C image of the IMEC staircase doping standard. The sample was measured using a two-pass method with no applied bias. The data are collected line by line; the first line is in contact mode, and the second pass is at a height 100 nm above the sample surface. The difference image is shown in Fig. 5(a). An average profile is shown in Fig. 5(b). The resulting profile shows excellent correlation to the IMEC published doping concentration data. The average profile graph (Fig. 5b) highlights where the average sMIM-C value was calculated for the graph in Fig. 5(c), plotting the measured sMIM-C versus known doping concentration.

Due to the very linear response of the sMIM-C versus log doping concentration, one can use the corresponding

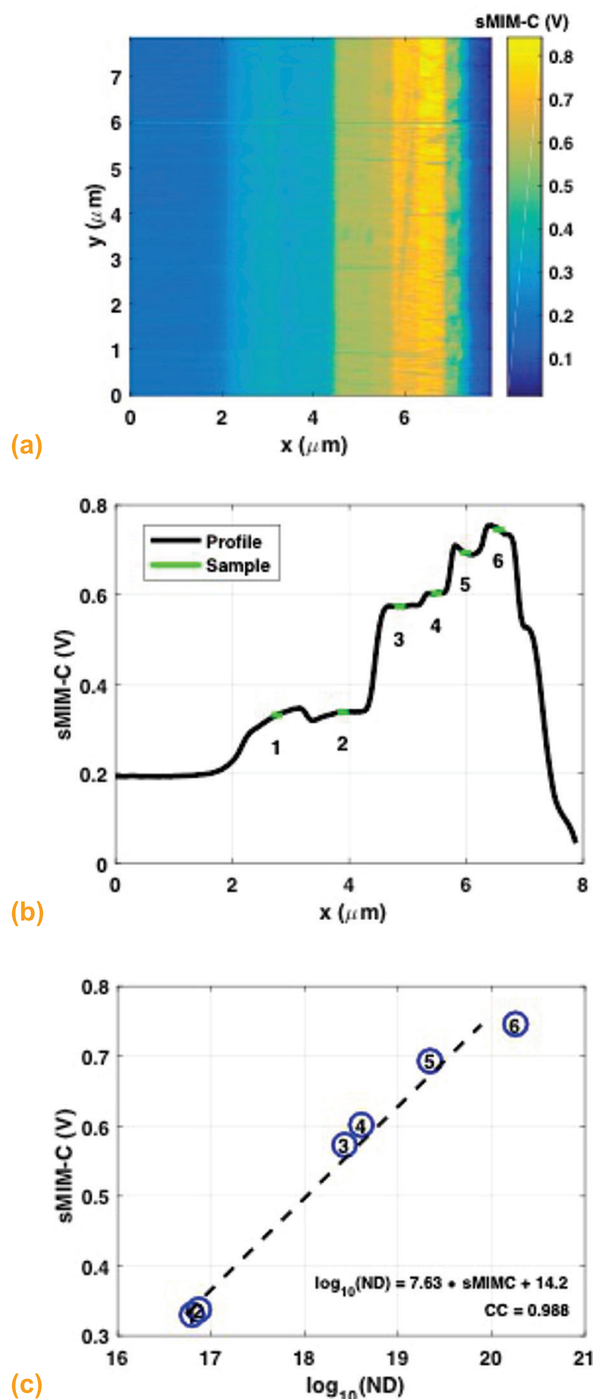

Fig. 5 **(a) Processed sMIM-C image of an *n*-type IMEC staircase. (b) Average profile with "calibration samples" highlighted in green. (c) Plot of sMIM-C calibration values versus published values of log doping. The linear fit is a calibration that can be applied to subsequent unknown doped samples.**

curve (Fig. 5c) as the calibration to convert sMIM-C measured on a device sample to log doping.[10]

Figure 6(a) presents the results of nano-C-V curves from the IMEC staircase, verifying that the nanoscale response matches the theory discussed in the introduction of this article. This "image" is from multiple sMIM scans over the same 8-µm-length line on the sample, collected as the bias voltage scans from 0 to 2.5 V. The demarcations of the doped regions are marked with vertical white lines, separated by exactly the widths of the regions published by IMEC for this sample. The data for the six C-V curves in Fig. 6(b) were taken from the vertical dashed black lines, which are placed exactly midway between the white lines. The C-V curves were shifted so they all have the same sMIM value at the most positive voltage, quite deep into accumulation. These empirical C-V curves for *n*-type silicon closely resemble the mirror images of the theoretical C-V curves for a *p*-type silicon, as they should. (The sMIM-C is proportional to the admittance at the tip/sample interface and therefore to the capacitance.) Figure 6(c) shows the sMIM-C values from the C-V curves in Fig. 6(b) at the tip-sample voltage with the highest doping sensitivity (0.96 V), and they vary linearly with log doping density over approximately 4 orders of magnitude. The derived linear calibration has the formula log(ND) = 1.83 × sMIM-C + 19.9, with a correlation coefficient of 0.972.

sMIM REFERENCE APPLIED TO A GaN DEVICE

This section extends the methods discussed previously on doped silicon systems to III-V semiconductor materials. An *n*-type GaN staircase reference sample was prepared using an *n*-type GaN subtrate and growing four epitaxial layers with varying doping levels. Two of the steps, 2 and 5, have the same doping concentration, as shown in Fig. 7(b). The sample was independently measured using secondary ion mass spectrometry (SIMS) to verify the doped step values, and these values were used for calibration. Figure 7(a) shows the sMIM-C image, with roughly vertical regions representing the individual steps. Using the technique described previously, an average profile of the steps is used to extract the sMIM step value (Fig. 7b), which is then plotted versus log doping to establish the calibration curve (Fig. 7c).

After calculating the calibration curve on the calibration sample, it can now be applied on an "unknown" GaN device to convert the sMIM to units of log doping concentration. The test device is a multilayer structure with both *n*- and *p*-type doped regions. This article concentrates on the *n*-type regions, because the calibration staircase is *n*-type only.

Figure 8(a) shows a cross-sectional schematic of the "unknown" device. The schematic identifies three regions of interest on the sample that are *n*-type doped regions: the reference region, L1, and L2. Figure 8(b) shows an

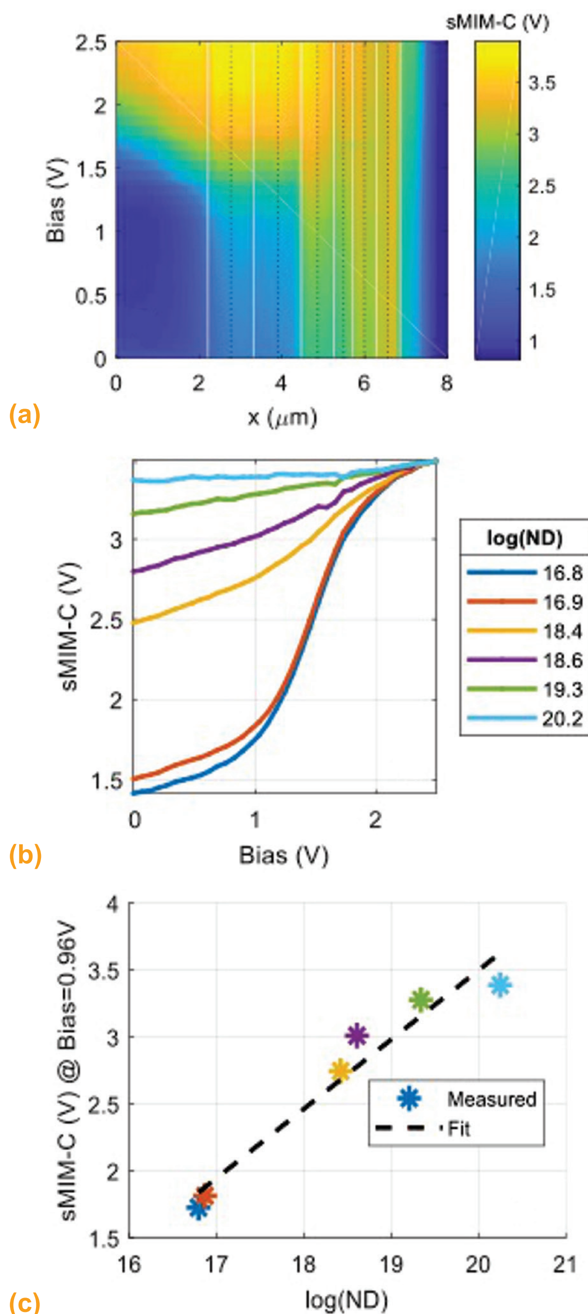

Fig. 6 **(a) Image of an 8 µm line scanned repeatedly while the bias voltage swept from 0 to 2.5 V. The vertical white lines demarcate the doped regions in this cross-sectional sample. The vertical dotted black lines indicate where values were extracted to give C-V curves. (b) C-V curves extracted from (a). The curves have been shifted vertically so they meet at bias = 2.5 V, deep into accumulation. (c) Calibration from sMIM-C to log(ND) at bias = 0.96 V, where sMIM-C has the most doping contrast**

sMIM-C image of the "unknown" device. The same three regions of interest are marked with dotted lines and labeled. The image is converted to units of log doping concentration after applying the calibration curve from Fig. 7(c).

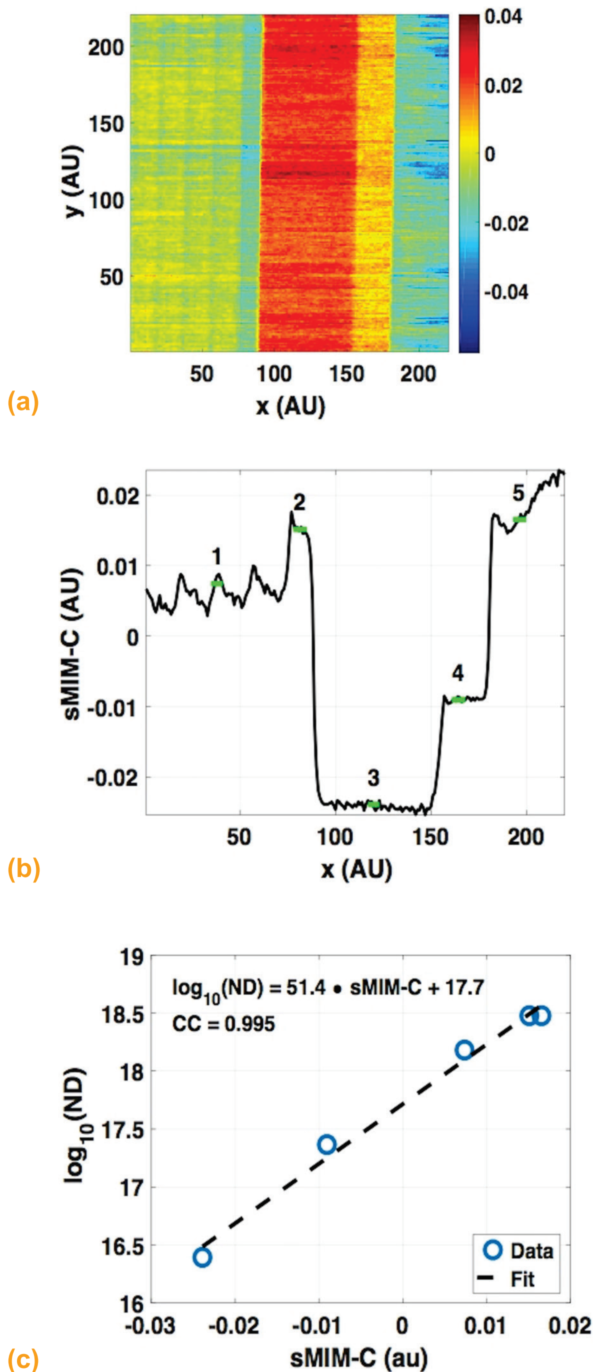

Fig. 7 **Measurement of a GaN epilayer *n*-type doped staircase. (a) sMIM-C image. (b) Average profile of the aligned image, with the highlights showing calibration values. (c) sMIM-C in millivolts versus doping concentration in log units. The graph shows good linearity over the range of doping and demonstrates the linear relationship of sMIM-C versus log(ND) for a nonsilicon semiconductor material.**

Figure 8(c) is the average profile extracted from the sMIM-C image in Fig. 8(b). The "reference region" of the "unknown" device has the same doping concentration as step 3 of the calibration sample. The common value allows compensation for the potential offsets that may occur due to system drift or systematic errors during the measurements. The calibration curve doping concentration value is shifted to pass through the reference value on the device sample and then applied to the whole profile to calculate doping concentrations.

The comparison of the nominal values with the calibrated sMIM values shows that the ratio of L1 to L2 is 2.0 for the SIMS and 1.3 for the sMIM, respectively. The result shows that sMIM is sensitive to the doping concentration difference in the two regions, differing by a factor of 2. The measured values are lower than the SIMS reference values. The authors speculate that the variation can be caused by

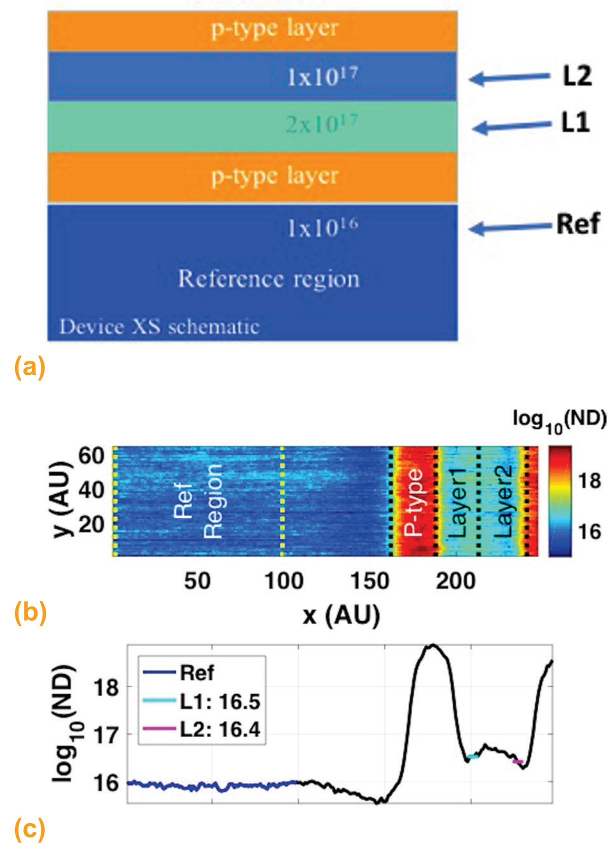

Fig. 8 **(a) Cross-sectional schematic of a GaN device. The sample is labeled with nominal doping values independently obtained by SIMS measurement to verify the nominal doping levels before cross sectioning and measuring with sMIM. (b) sMIM image of the "unknown" sample with color scale converted to *n*-type doping concentration using the calibration data from Fig. 7. (c) Average profile of the sMIM data, where the Ref line is highlighted. The 1×10^{16} region has the same doping concentration as step 3 of the reference sample.**

the difference in measured doping concentration, because SIMS measures the implanted doping density, and sMIM-C measures the activated doping concentration, as well as possible systematic variation during the measurements that could account for the discrepancy. It is expected for GaN that the activated doping concentration would be lower than the implanted density.

The application of sMIM to a cleaved cross-sectional GaN device sample demonstrates the robustness of the method and the flexibility to measure doping levels on an unknown device sample using a known staircase for calibration of III-V materials. Further refinements are ongoing.

SUMMARY

Scanning microwave impedance microscopy as a new mode for electrical measurements integrated to an AFM can address the needs of the semiconductor and failure analysis communities by providing increased sensitivity to investigate semiconductor devices for current and next-generation technologies. Adoption of sMIM will enhance the available toolkit, especially in addressing quantification of doped semiconductors and dielectric materials.

This article presents examples of some of the benefits of the sMIM technology: linear correlation to the log of dielectric coefficient; linear response to the log of doping concentration; visualization of metal, doped materials, and dielectrics in the same image; nanoscale C-V curves; and quantification of doping concentration on different classes of semiconductor materials.

The AFM probes present specific challenges due to their shape and wear during measurements. This article presented the results validating the authors' models with comparison of the classic one-dimensional MOS model with a three-dimensional finite-element analysis cone-shaped model, confirming that using an AFM probe as an electrode for nanoscale C-V curves is different from those acquired with parallel-plate geometry but has similar potential for yielding quantitative characterizations. The article also showed that C-V curves can be measured from doped semiconductors and that they are consistent with what is predicted by theory for this type of three-dimensional geometry.

The article showed that single-bias images and single-point C-V measurements on an IMEC *n*- and *p*-type doped staircase sample are consistent and therefore can be used together to give an enhanced, quantitative view of a sample's doping state. In addition, it has been shown that sMIM measurements on III-V semiconductor materials and silicon behave very similarly, so methods developed for the latter can be applied to the former; namely, a calibration from a known staircase sample can be applied to the sMIM image of an "unknown" device sample to estimate doping concentrations.

REFERENCES

1. Y. Yang, E.Y. Ma, Y.-T. Cui, A. Haemmerli, K. Lai, W. Kundhikanjana, N. Harjee, B.L. Pruitt, M. Kelly, and Z.-X. Shen: "Shielded Piezoresistive Cantilever Probes for Nanoscale Topography and Electrical Imaging," *J. Micromech. Microeng.,* 2014.
2. N. Duhayon, T. Clarysse, P. Eyben, W. Vandervorst, and L. Hellemans: "Detailed Study of Scanning Capacitance Microscopy on Cross-Sectional and Beveled Junctions," *J. Vac. Sci. Technol. B: Microelectron. Nanometer Struct.,* 2002, *20*(2).
3. N. Duhayon, P. Eyben, M. Fouchier, T. Clarysse, W. Vandervorst, D. Álvarez, S. Schoemann, et al.: "Assessing the Performance of Two-Dimensional Dopant Profiling Techniques," *J. Vac. Sci. Technol. B: Microelectron. Nanometer Struct.,* 2004, *22*(1).
4. S. Friedman, O. Amster, and Y. Yang, "Recent Advances in Scanning Microwave Impedance Microscopy (sMIM) for Nano-Scale Measurements and Industrial Applications," *Proc. SPIE,* 2014, *9173*, id. 917308.
5. J.R. Matey and J. Blanc: "Scanning Capacitance Microscopy," *J. Appl. Phys.,* 1985, *57*(5), pp. 1437-44.
6. B. Drevniok, St.J. Dixon-Warren, O. Amster, S.L. Friedman, and Y. Yang: "Extending Electrical Scanning Probe Microscopy Measurements of Semiconductor Devices Using Microwave Impedance Microscopy," *Proc. 41st Int. Symp. Test. Fail. Anal. (ISTFA),* 2015, p. 77.
7. Z.Y. Wang et al.: "Evanescent Microwave Probe Measurement of Low-k Dielectric Films," *J. Appl. Phys.,* 2002, *92*, p. 808.
8. E.Y. Ma, M.R. Calvo, J. Wang, B. Lian, M. Mühlbauer, C. Brüne, Y.-T. Cui, et al.: "Unexpected Edge Conduction in Mercury Telluride Quantum Wells under Broken Time-Reversal Symmetry," *Nature Commun.,* 2015.
9. E. Seabron, S. MacLaren, X. Xie, S.V. Rotkin, J.A. Rogers, and W.L. Wilson: "Scanning Probe Microwave Reflectivity of Aligned Single-Walled Carbon Nanotubes: Imaging of Electronic Structure and Quantum Behavior at the Nanoscale," *ACS Nano,* 2015.
10. E.Y. Ma, Y.-T. Cui, K. Ueda, S. Tang, K. Chen, N. Tamura, P.M. Wu, J. Fujioka, Y. Tokura, and Z.-X. Shen: "Mobile Metallic Domain Walls in an All-In-All-Out Magnetic Insulator," *Science,* 2015, *350*(6260), p. 538.
11. A. Tselev, P. Yu, Y. Cao, L.R. Dedon, L.W. Martin, S.V. Kalinin, and P. Maksymovych: "Microwave A.C. Conductivity of Domain Walls in Ferroelectric Thin Film," *Nature Commun.,* May 2016, pp. 1–9, doi:10.1038/ncomms11630.
12. H.P. Huber, I. Humer, M. Hochleitner, M. Fenner, M. Moertelmaier, C. Rankl, A. Imtiaz, et al.: "Calibrated Nanoscale Dopant Profiling Using a Scanning Microwave Microscope," *J. Appl. Phys.,* 2012, *111*(1).
13. St.J. Dixon-Warren and B. Drevniok: "Practical Quantitative Scanning Microwave Impedance Microscopy," *Proc. 42nd Int. Symp. Test. Fail. Anal. (ISTFA),* 2016.
14. W.S. Hu, J.H. Lee, M.H. Kao, H.W. Yang, P. Dewolf, and O. Amster: "Device Dielectric Quality Analysis and Fault Isolation at the Contact Level by Scanning Microwave Impedance Microscopy," *Proc. 42nd Int. Symp. Test. Fail. Anal. (ISTFA),* 2016.
15. Y.L. Yang, K.J. Lai, Q.C. Tang, W. Kundhikanjana, M. Kelly, Z.X. Shen, and X. Li: "A Shielded Cantilever-Tip Microwave Probe for Micro/Nano Surface Imaging of Conductive Properties," *2011 IEEE 24th Int. Conf. Micro Electro Mech. Syst. (MEMS),* 2011.
16. K. Lai, W. Kundhikanjana, M.A. Kelly, and Z.X. Shen: "Calibration of Shielded Microwave Probes Using Bulk Dielectrics," *Appl. Phys. Lett.,* 2008.
17. R. Pierret, *Semiconductor Device Fundamentals,* 2nd ed., Pearson, 1995.

(continued on page 20)

 (continued from page 18)

ABOUT THE AUTHORS

Oskar Amster has 20 years of experience working with analytical instruments and metrology tools. His background is in applications development, strategic marketing, and product development. He has extensive experience working in atomic force microscopy, stylus profilers, and optical profiler instruments. Prior to joining PrimeNano, Inc., Oskar was Product Marketing Manager at KLA-Tencor and held positions at Ambios Technology, Ametek Taylor Hobson, Multiprobe, Micron Force Instruments, and Topometrix. He has an M.S. in materials engineering and a B.S. in physics from California Polytechnic State University, San Luis Obispo.

Stuart Friedman has engaged in academic and industrial research in a variety of areas, including image processing, surface science, electron optics, bio-medical instrumentation, and bio-physical simulation. He currently serves as Chief Technology Officer of PrimeNano, Inc., a Silicon Valley instrumentation startup focused on commercial implementation of scanning microwave impedance microscopy for research and commercial applications. Before co-founding PrimeNano, Dr. Friedman founded and led a research and development and systems engineering consulting firm in Silicon Valley, helping transition complex systems to commercial reality for startups as well as Fortune 500 clients. Prior to that, he held research and development, systems architecture, and technical leadership roles at Gatan, Inc., Etec Systems, KLA-Tencor, MDS Sciex, and Signature Bioscience. Dr. Friedman holds a Ph.D. in applied physics from Stanford University, an M.Phil. in physics from Cambridge University, and a B.S.E. in engineering physics from Cornell University.

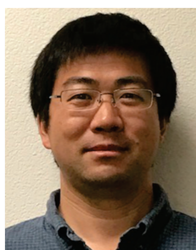

Yongliang Yang has been conducting research on scanning probe microscopy technology for the past five years. He has also spent more than 10 years doing research on MEMS devices. Before joining PrimeNano, Inc. in 2014 as a research and development scientist, Dr. Yang was a postdoctoral student at Stanford University, developing scanning microwave impedance microscopy (sMIM) technology and studying electrical properties of materials with sMIM. Dr. Yang has a B.S. degree from Peking University and a Ph.D. from the Chinese Academy of Sciences. He holds four patents and is the author of more than 40 publications.

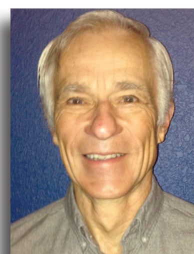

Fred Stanke has done research and development of metrology and inspection systems for a wide range of applications. For his Ph.D. dissertation at Stanford University, he developed ultrasonic metrology to nondestructively measure the grain sizes of metals. He did research with Schlumberger Limited on using ultrasound to inspect oil well casings for their capability to provide hydraulic isolation. At the startup Sensys Instruments, Dr. Stanke headed the technical team to develop an optical system using scatterometry to measure the critical dimensions of integrated circuits. He accompanied that product when Tokyo Electron Limited bought it to integrate into semiconductor clean tracks to improve and shorten the control loop for microlithography. At PrimeNano Inc., Dr. Stanke does research and development to allow scanning microwave impedance measurements to quantify properties such as the doping concentrations of semiconductors.